Dielectric Properties of Thermosetting Material Nanocomposites

Newton Luiz Dias Filho,[1] Hermes Adolfo de Aquino,[1] Denise Souza Pereira,[1] André H. Rosa[2]

[1]*Departamento de Física e Química, Unesp-Universidade Estadual Paulista, Av. Brasil, 56 – Centro, Caixa Postal 31, 15385-000 Ilha Solteira – SP, Brazil*
[2]*Departamento de Engenharia Ambiental, Unesp-Universidade Estadual Paulista, CEP 18087-180, Sorocaba, SP – Brazil*

Received 10 May 2006; accepted 27 January 2007
DOI 10.1002/app.26393
Published online 18 June 2007 in Wiley InterScience (www.interscience.wiley.com).

ABSTRACT: The dieletric relaxation properties of thermosetting material nanocomposites based on spherosilicate nanoplatforms were studied from room temperature to 170°C, varying the frequency from 10 to 1000 KHz. Permittivity (ε′), dielectric loss (ε″), and activation energy (E_a) were calculated. The results of dielectric relaxation were confirmed by those of the final properties. The dielectric loss amplitude decreases with increasing ODPG content until about 70–73 wt % and slightly increases at higher ODPG content. This means that the increasing of the ODPG content in the composite samples decreases the number of pendants groups and/or increases crosslink density, causing decreased motion of organic tethers, and subsequently decreasing of the dipolar mobility. The results of apparent activation energy, fracture toughness and tensile modulus mechanical properties show the same profile with respect to ODPG content, in the sense that they exhibit maxima around 70 wt % ODPG. For the ODPG/MDA composites, this formulation of 70 wt % ODPG containing excess of amine is not composition where the highest crosslinked density is reached. This implies that the best mechanical properties and E_a are provided by some degree of chain flexibility. © 2007 Wiley Periodicals, Inc. J Appl Polym Sci 106: 205–213, 2007

Key words: dieletric relaxation; thermoset material; nanocomposite; spherosilicate

INTRODUCTION

Polyhedral oligomeric silsesquioxanes (POSS), $(RSiO_{1.5})_n$ with $n = 6, 8, 10. . . .$, are nanoplatforms with 1–8 reactive or nonreactive organofunctional groups (R) anchored to the possible eight vertexes of the cubic silsesquioxane. Octahedral POSS ($n = 8$) are the most important members of this family.[1–3]

POSS with $n = 8$ are usually synthesized via catalyzed hydrosilylation of organic molecules containing terminal vinyl groups with 1,3,5,7,9,11,13,15 -octa[hydridodimethylsiloxy] pentaciclo $[9.5.1.1^{3,9}.1^{5,15}.1^{7,13}]$ octasilsesquioxane, $[(HMe_2SiOSiO_{1.5})_8]$, using Pt(dcp). In these POSS, the eight organic functional groups (R) are anchored to the vertexes of the cube via $O(SiMe_2$-(spacer) linkages. POSS can be incorporated into thermosetting or linear polymers to improve their thermal and mechanical properties. The use of such nanosized POSS in the preparation of an organic polymer by polymerization at one or more of the eight corner groups in the POSS macromer, can lead to nanocomposite materials.[4–9]

Nanocomposite materials can offer novel properties, such as significant improvements in tensile modulus, fracture toughness, thermal and oxidation resistance, and reduced flammability, that can only be explained by extensive organic–inorganic interfacial interactions.[10–12]

Recently, the preparation and study of several organic–inorganic hybrid composites based on several types of octa-functional POSS has been reported.[4–12] In these materials, the cubic silica core is defined as rigid nanoplatform in which eight organic functional groups are anchored to the vertexes of the cube. The cubic silica cores are ''hard particles'' rigid with 0.53 nm diameter and a spherical radius of 1–3 nm including peripheral organic units. In these materials the cubes can be connected to one another by organic components with known architecture and lengths of the order of 3–5 nm, forming composites with completely defined interfacial component between organic and inorganic phase. The dimensions of the organic connectors between mono-dispersed cubic silsesquioxanes with size at nanometer scale are within the dimensions normally attributed to interphase materials that form in macroscopic composites.

Dielectric analysis (DEA) technique detects changes in ionic and dipolar mobilities of a material when it is subjected to an alternating electric field.[12,13] It has been used to investigate the relaxational behavior of organic materials for more than half a century.[14–20]

Correspondence to: N. L. D. Filho (nldias@dfq.feis.unesp.br).
Contract grant sponsors: FAPESP, CNPq.

In the present work, the dielectric relaxation behavior of a thermosetting material, obtained from curing of 1,3,5,7,9,11,13,15-octa[dimethylsiloxypropylglycidylether] pentaciclo [9.5.1.1^{3,9}.1^{5,15}.1^{7,13}] octasilsesquioxane, [(glycidylMe$_2$SiOSiO$_{1.5}$)$_8$] (ODPG), which is a epoxy resin based on cubic silsesquioxane, in presence of the curing agent (hardener) methylenedianiline (MDA), was studied.

As the most important epoxy resin are oligomers of diglycidyl ether of bisphenol A, we have chosen the allyl glycidyl ether to be added to the octa[hydridodimethylsiloxy] octasilsesquioxane in the present work, resulting an epoxy resin based on cubic silsesquioxane, or more specifically, a POSS. For the same reason, the methylenedianiline has been chosen as the curing agent.

Dielectric relaxation technique allows to probe the molecular mobility of the organic phase of the organic–inorganic hybrid composites. In this context, both frequency and temperature are varied, so that a wide range of molecular mobility can be investigated. Since the aim of this work is to see how the presence of organic functional groups affects the relaxational behavior of the composite matrix, experimental work was carried out on different formulations. The samples were prepared in a similar way, allowing an easy comparison among the results obtained for different ODPG content.

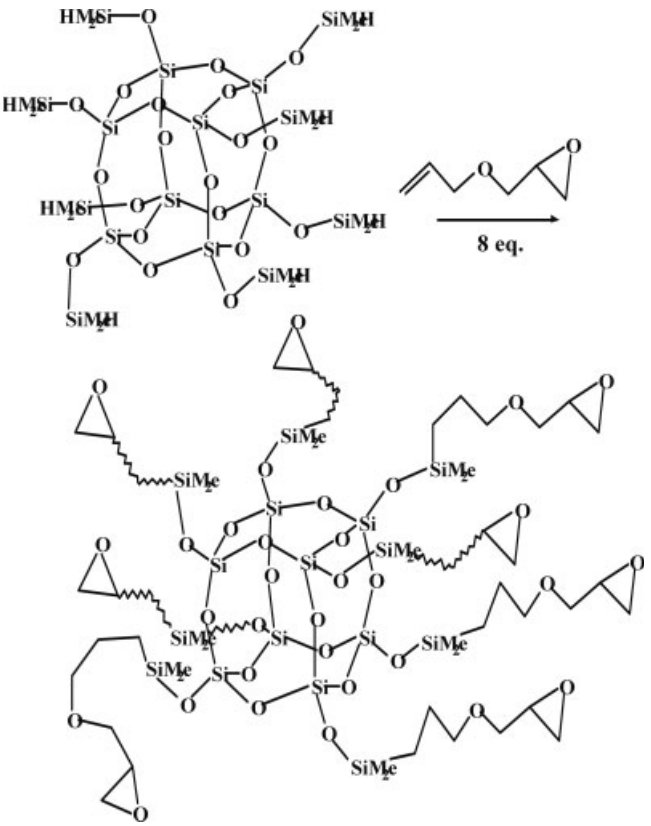

Figure 1 Reaction of preparation of the 1,3,5,7,9,11,13,15-octa [dimethylsiloxypropyl glycidylether] pentaciclo [9.5.1.1^{3,9}.1^{5,15}.1^{7,13}] octasilsesquioxane (ODPG).

EXPERIMENTAL

Materials

Tetraethoxysilane [Si(OEt)$_4$], tetramethylammonium hydroxide [(CH$_3$)$_4$NOH], dimethylchlorosilane [HSi(CH$_3$)$_2$Cl], allyl glycidyl ether, and platinum dicyclopentadieno [Pt(dcp)], triphenylphosphine and methylenedianiline were purchased from Aldrich Chemical Company and used as received. Hexane and methanol was purchased from Lancaster Synthesis Company and used without further purification.

Synthesis

The synthesis of the 1,3,5,7,9,11,13,15-octa[dimethylsiloxypropylglycidylether] pentaciclo [9.5.1.1^{3,9}0.1^{5,15} 0.1^{7,13}] octasiloxane, [(glycidylMe$_2$SiOSiO$_{1.5}$)$_8$] (ODPG) followed a procedure previously reported.[11] A schematic representation of this reaction is showed in Figure 1.

To a 500-mL Schlenk flask equipped with a magnetic stir bar and a condenser, was added 120.0 g (0.1178 mol) octahydrido spacer cube, [HMe$_2$-SiOSiO$_{1.5}$]. The flask was evacuated and refilled with N$_2$ gas three times at 50°C. Then 132.0 mL (0.99 mol) allyl glycidyl ether was added to the solution followed by 0.3 mL of 2.0 m*M* solution of platinum dicyclopentadieno [Pt(dcp)] and the reaction was heated at 90°C. Triphenylphosphine, 10 mg, was then added to deactivate the [Pt(dcp)] catalyst and the toluene solvent was removed by rotary-evaporation. Yield: 210 g (91% of theoretical).

^{1}H-NMR (CDCl$_3$): δ C*H*$_2$O(CH$_2$)$_3$ diastereotopic 3.55, 3.30 (dd, *J* = 3,27 Hz, 8H) (due to peak overlap, all resonances between 3.34 and 3.16 are integrated as two peaks, 24H), 3.30, 3.28 (dd, *J* = 2,89 Hz), SiCH$_2$CH$_2$C*H*$_2$O 3.18 (m, 8H), OCH$_2$C*H* (epoxy) 2.93 (m, 8H), C*H*$_2$ (epoxy) diastereotopic 2.58 (dd, 8H), 2.40 (dd, 8H), SiCH$_2$C*H*$_2$CH$_2$O 1.48 (m, 16H), SiC*H*$_2$CH$_2$CH$_2$O 0.47 (m, 16H), (C*H*$_3$)$_2$SiCH$_2$ 0.00 ppm (s, 48H).

^{13}C-NMR (CHCl$_3$): δ SiCH$_2$CH$_2$CH$_2$O 74.29, *C*H$_2$O(CH$_2$)$_3$ 71.86, OCH$_2$CH (epoxy) 51.11, *C*H$_2$ (epoxy) 44.35, SiCH$_2$CH$_2$*C*H$_2$O 23.59, SiCH$_2$CH$_2$*C*H$_2$O 13.93, (*C*H$_3$)$_2$SiCH$_2$ 0.00 ppm.

^{29}Si-NMR (C$_6$D$_6$): δ (CH$_3$)$_2$*Si*CH$_2$ −7.3, *Si*OSi(CH$_3$)$_2$ CH$_2$ −129.4 ppm.

SEC, M_n = 1850, M_w = 1898, PDI = 1.02, calculated M_w = 1931 g/mol.

Fourier transform infrared spectra (FTIR) (neat film, cm^{-1}): ν C—H = 3035, 2962, 2934, 2874 (m); ν Si—H = 2142 (m); ν Si—CH$_3$ e ν C—O = 1250–1260 (s); ν Si—O = 1095 (versus); δ C—O—C = 902 (s).

TABLE I
Formulations for ODPG/MDA Composites

ODPG wt %	MDA wt %	ϕ[a]	Molar ratio MDA/ODPG	ε' (at 50 KHz)	ε'' (at 50 KHz)	T_p (°C) (at 50 KHz)	E_a KJ mol^{-1}	E[b] G Pa	K_{1C}[b] MPa.m$^{1/2}$
95	5	3.90	0.51					0.02	
91	9	2.07	0.96					0.06	
87	13	1.37	1.46					0.70	
83	17	1.00	1.99	8.99	0.19	13	241	1.00	0.45
80	20	0.82	2.44						0.53
79	21	0.77	2.59						0.60
77	23	0.69	2.91	7.12	0.17	35	322	1.28	
73	27	0.55	3.60	7.80	0.11	102	362		0.80
70	30	0.48	4.18				479	1.68	1.25
68	32	0.44	4.58						1.35
67	33	0.42	4.79	7.90	0.19	93	368	1.70	
63	37	0.35	5.72	8.40	0.37	56	264		
60	40	0.31	6.49				253	0.74	
57	43	0.28	7.10	9.49	0.54	45	248		
55	45	0.25	7.96					0.17	
50	50	0.20	9.74					0.03	
40	60	0.14	14.62					0.02	

[a] In formulating samples, the molar ratio ϕ is defined as the ratio of epoxy ring to amine hydrogen (ϕ = number of epoxy rings in ODPG/number of amine hydrogen in MDA).
[b] Each data point represents an average of at least five samples.

Curing process

The compositions of samples were shown in Table I.

ODPG is a viscous liquid and MDA is solid at room temperature. The structures of the ODPG and MDA are shown in the Figures 1 and 2, respectively. A general schematic representation of composites with discontinuous organic–organic phases from cubic silsesquioxane is shown in Figure 3.

In the present investigation, samples having different amount of ODPG were prepared. In formulating samples, the molar ratio ϕ is defined as ϕ = no. of epoxy rings in ODPG/no. of amine hydrogen in MDA = 8 × (no. of ODPG)/4 × (no. of MDA). Thus, when $\phi = 1$, the two components are mixed at stoichiometric amount of 83 wt % of ODPG and 17 wt % of MDA.

For curing optimization tests, samples were cured at different temperatures and times to study the cure condition. ODPG/MDA samples were cured in the temperature range of 100–200°C and for periods of 2–12 h. It was performed in two steps curing cycle tests and not any improvement was observed in the mechanical properties of the samples. It was determined that for ODPG/MDA, curing for 10 h at 150°C was sufficient for reproducible modulus and fracture toughness. Then, in the present study curing for 10 h at 150°C was adopted for the composites ODPG/MDA.

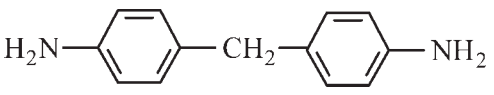

Figure 2 Structure of the methylenedianiline (MDA).

ODPG and MDA were weighed into an aluminum pan with a diameter of 61.5 mm and depth of 18 mm and mixed by hand at room temperature. The mixture was then put into an oven preheated to ~150°C under vacuum. After degassing for 10–15 min and no more bubbles emerged from the mixture, the content was transferred to an aluminum mold preheated to 150°C. The filled mold was placed in an oven and heated under nitrogen for 10 h at 150°C for curing the mixture. After the mold cooled, the sample was removed and kept in a sealed desiccator before the mechanical tests were performed.

Mechanical testing

Samples removed from the aluminum mold had rough edges due to the overflow of polymer. These edges were polished using a polish wheel with 120-grit SiC paper. After polishing, the samples were ready for mechanical testing. The elastic moduli (E) data were obtained using an Instron 4502 screw driven mechanical testing machine. The dimensions of each sample were determined by measuring the width and thickness at three points along the gauge length prior to the test. These were used to calculate the averages of width and thickness for each sample.

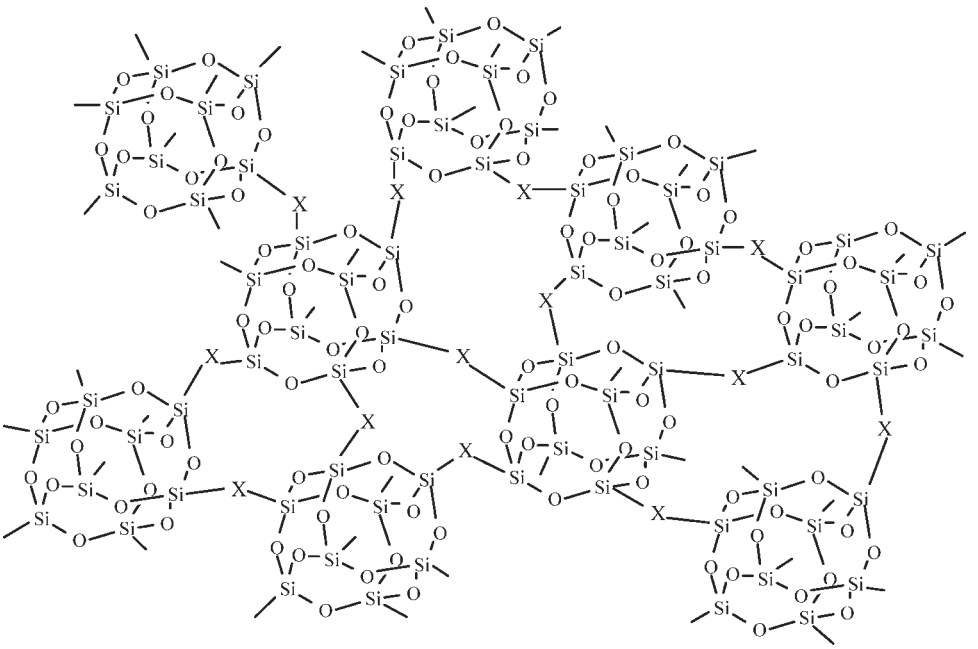

Figure 3 Scheme of a general representation of composites with discontinuous organic–organic phases from cubic silsesquioxane. X = links between cubes.

The elastic moduli were obtained following ASTM standard [No. E111(1997)].

The critical stress intensity factor was obtained following ASTM standard [No. E399(1990)].

NMR and FTIR analyses

Solution NMR Analyses. All ^{1}H- and ^{13}C-NMR analyses were done in $CDCl_3$ and recorded on a BRUKER DRX 400 spectrometer. ^{13}CNMR spectra were obtained at 100.6 MHz using a 27,027 Hz spectral width and a relaxation delay of 0.6 s. ^{1}H-NMR spectra were collected at 400.1 MHz, using a 3591 Hz spectral width, and a relaxation delay of 1 s.

Solid state NMR analyses. All ^{29}Si-NMR (59.5 MHz) and ^{13}C-NMR (75.4 MHz) solid state analyses were recorded on a Varian INOVA 300 spectrometer. The samples were packed in zirconia rotors and spun at the magic angle at 4500 Hz, after a relaxation delay of 10.0 and 6.0 s for ^{29}Si and ^{13}C, respectively. All chemical shifts are reported in units (ppm) using TMS as external reference.

FTIR spectra were recorded on a Nicolet 5DXB FT-IR 300 spectrometer. About 600 mg of KBr were ground in a mortar and pestle, and a sufficient quantity of the solid sample was ground with KBr to produce a 1 wt % mixture resulting in pellets. Liquid samples were cast on salt plates. A minimum of 32 scans was collected at a resolution of 4 cm^{-1}.

Dielectric measurements

Dieletric relaxation experiments were performed using a Hewlett–Packard Impedance and Gain Phase Analyser 4192A. All films had a layer of aluminum evaporated on both surfaces to serve as electrodes. Sample thickness of about 1 mm was used. The aluminum-coated films were installed in a closed ($\sim 10^{-2}$ torr vacuum), temperature controlled cell of parallel plate geometry. The capacitance, C, and loss factor, tan δ, of the samples were measured over a frequency range from 10 to 1000 KHz, from room temperature to 170°C.

Dynamic mechanical analysis

Dynamic mechanical analysis (DMA) was performed on cured samples using a Netzsch DMA 242 instrument operating at 1 Hz in the three-point bending mode at a heating rate of 5°C/min. The dimensions of the specimens were $\sim 3.1 \times 10 \times 100$ mm^3. Dynamic mechanical spectra were obtained from -50 to 200°C.

RESULTS AND DISCUSSION

Dieletric relaxation technique allows to study changes in ionic and dipolar mobilities of a thermoset material when it is subjected to an alternating electric field.[14–20]

In DEA, the capacitance and conductance of a material can be measured as a function of time, temperature, and frequency. This allows the determination of electrical polarization and conduction of the material.

The real (ε') and imaginary (ε'') parts of the dielectric function are determined from the measured

quantities according to:

$$\varepsilon' = Cd/AC_o \quad (1)$$

$$\varepsilon'' = \varepsilon' \tan \delta \quad (2)$$

where C is the parallel capacitance, d is the initial film thickness, A is the electrode area, and C_o is the permittivity of free space ($C_o = 8.85 \times 10^{-12}\ F/m$). ε' is the permittivity and measures the polarization of the material; ε'' is the dielectric loss and is related to the energy loss and the conductive nature of the sample.

In an electric field, dipoles tend to align themselves along the direction of the field, while ions move toward the electrodes and form layers. Before the curing reaction starts, dipoles and ions can move freely. After the curing process, ions lose their translational mobility and dipoles lose their rotational mobility. Such change in ionic and dipolar mobilities leads to the development of a peak in the dielectric loss (ε'') curve.

The dielectric relaxation of conventional epoxy-amine systems has been discussed at length by Fitz and Mijovic.[18] The α process is associated with segmental motions of the terminal epoxy groups while the β process results from the localized motions. In these conventional systems, a single $\alpha\beta$ relaxation first appears in the early stage of reaction, located in the high megahertz range. The $\alpha\beta$ relaxation peak broadens with the progress of chemical reactions and separates into two peaks: α which shifts to lower frequencies and longer relaxations times, and a second peak at high frequency (megahertz range) of diminishing intensity, but essentially unchanging relaxation time.

The ODPG/MDA composites investigated in this work were obtained from curing of the nonconventional epoxy resin denominated 1,3,5,7,9,11,13,15-octa[dimethyl siloxypropylglycidylether] pentaciclo [9.5.1.1^{3,9}.1^{5,15}.1^{7,13}] octasilsesquioxane in presence of methylenedianiline. Dielectric relaxation results in the temperature range 25–170°C, varying the frequency from 10 to 1000 KHz, are shown in Figure 4(a–f) for the ODPG/MDA composites. Figures 4(a–c) show that the peak position in the permittivity (ε') curves is frequency-dependent. The ε' showed only one wide absorption band, which shifts to higher frequency with increasing temperature, indicating that the process is actived termically. From Figure 4(a–c), we can observe for all studied frequencies that the height of the ε' peak maximum decreases with increasing ODPG content until about 75–77 wt %, then sharply increases until 83 wt %. The Table I shows the ε' maximum peak values as a function of ODPG content for the ODPG/MDA composites at 50 KHz.

The Figure 5(a–c) plots the dielectric loss (ε'') as a function of temperature for frequency in the range

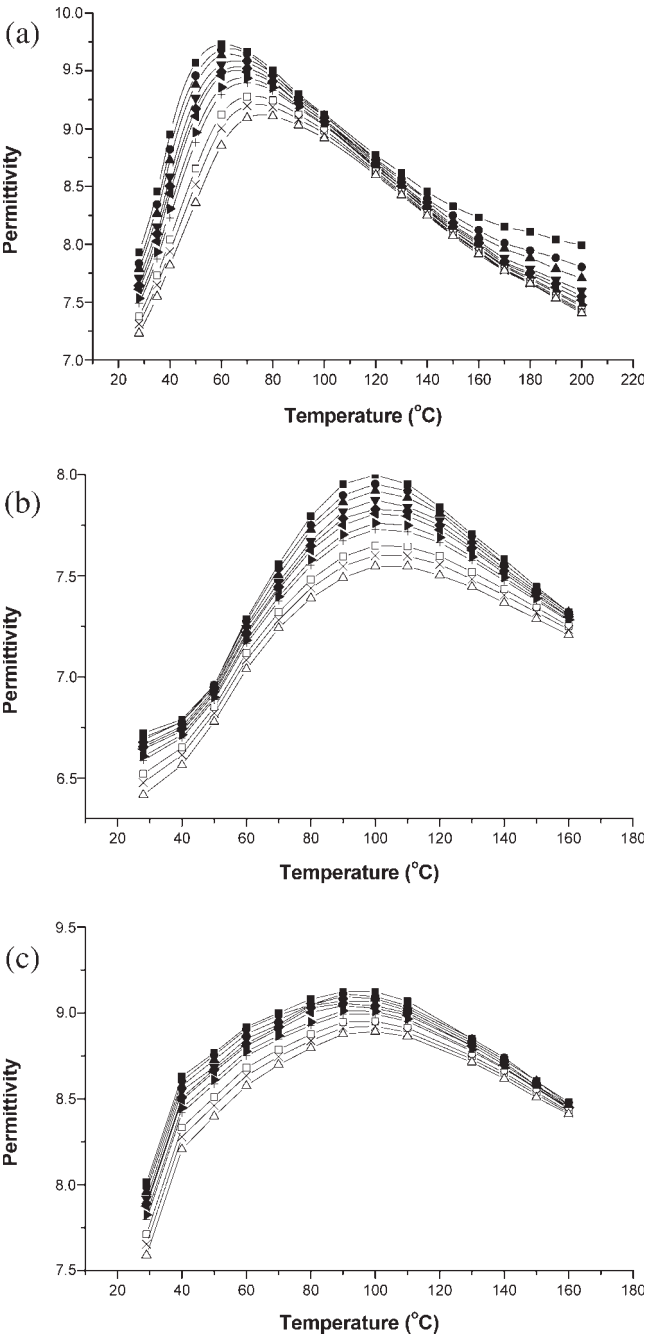

Figure 4 Permittivity (ε') as a function of temperature at several frequencies and ODPG contents: (a) 57 wt %; (b) 73 wt %; (c) 83 wt %. ■ 10 KHz; ● 15 KHz; ▲ 20 KHz; ▲ 30 KHz; ◆ 40 KHz; ◀ 50 KHz; ▶ 76 KHz; + 100 KHz; □ 200 KHz; × 302 KHz; △ 501 KHz.

of 10–000 KHz. The dielectric loss show the usual shape, reaching a maximum whose peak position shifts to higher temperature with increasing frequency. The ε'' maximum peak amplitude decreases with increasing ODPG content until about 70–73 wt % and slightly increases at higher ODPG content. The Table I presents the ε'' maximum peak values as a function of ODPG content for the ODPG/MDA

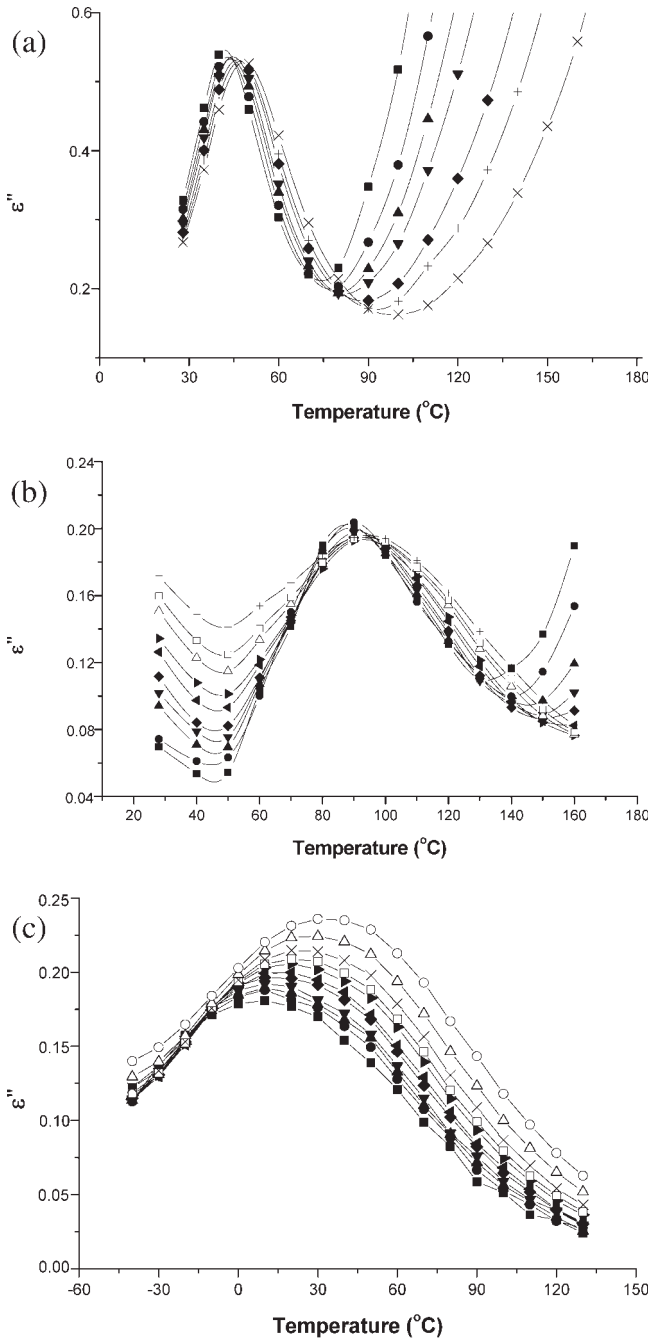

Figure 5 Dielectric factor (ε″) as a function of temperature at several frequencies and ODPG contents: (a) 57 wt %; (b) 73 wt %; (c) 83 wt %. ■ 15 KHz; ● 20 KHz; ▲ 30 KHz; ▲ 40 KHz; ◆ 50 KHz; ◀ 76 KHz; ▶ 100 KHz; △ 151 KHz; □ 200 KHz; + 300 KHz; × 501 KHz; ○ 1 MHz.

composites at 50 KHz. The temperature of the ε″ maximum peak position (T_p) increases with the increasing of ODPG content, reaching maximum values for compositions in the range of 67 and 73%, and then it decreases sharply at higher ODPG content (Table I). For the other studied frequencies the curves of the variation in the intensity and temperature position of the ε″ maximum as a function of OG content show the same behavior.

The conclusion we may draw from these results is that with excess increasing of the MDA content (''Excess'' MDA is used for $\phi < 1.0$; ODPG content < 83 wt %) in the composite samples increases the number of pendants groups (amount of the NH_2 dipolar groups) and/or decreases crosslink density, causing increased motion of organic tethers (links between cubes), and subsequently increasing of the dipolar mobility. The region with ODPG content higher than 70–73 wt % is very slightly affected by increased dipolar mobility, because it is in close proximity to the stoichiometric point ($\phi = 1.0$; 83 wt % ODPG). It is difficult to prepare samples with large excess of glycidyl units ($\phi > 1.0$), and the dielectric relaxation of these ODPG/MDA composites cannot be measured because of the viscous-like behavior, i.e., the sample bar begins to loss its solid integrity and becomes something like a very viscous material.

On the other hand, for composites ODPG/MDA samples with higher ODPG content (~80 wt % ODPG), at the lowest frequencies we see few upturns in the dielectric loss at high temperature, as result of increased dipolar mobility. This effect increases with decreasing of ODPG content involving higher frequencies. In samples with ODPG content low (~57 wt % ODPG), sharp upturns appear involving all range of frequency. This final sharp upturns in the dielectric loss is result of the increased dipolar mobility. This effect is dependent on increasing of the MDA content (providing source of polar NH_2 groups). Above 80 wt % ODPG, the content of polar NH_2 groups is very low, and this effect is not observed, i.e., there are fewer remaining dipoles able to respond to the field as time goes on.

In the range from 67 to 83 wt % ODPG we can see a different effect at low temperature. We can see upturns in the dielectric loss at low temperature, involving all frequency range. This effect becomes larger as the ODPG content increases from 67 to 83 wt % ODPG. Above 83 wt % ODPG this effect is not observed. It seems that the MDA excess decreasing (for $\phi > 0.45$; MDA content < 32 wt %) increases this effect by decreasing the number of pendants groups NH_2 and/or increasing crosslink density.

Assuming that the relaxation process can be modeled by an Arrhenius temperature dependence, the shift in the frequency of the loss peak maximum can be plotted as a function of reciprocal of the measurement temperature for several ODPG/MDA samples. The data can be fit to a straight line whose slope is the activation energy parameter for the α relaxation process. Figure 6 shows a set of Arrhenius plot obtained by plotting ln f versus $1/T_p$, where T_p is the peak maximum temperature of the dielectric loss

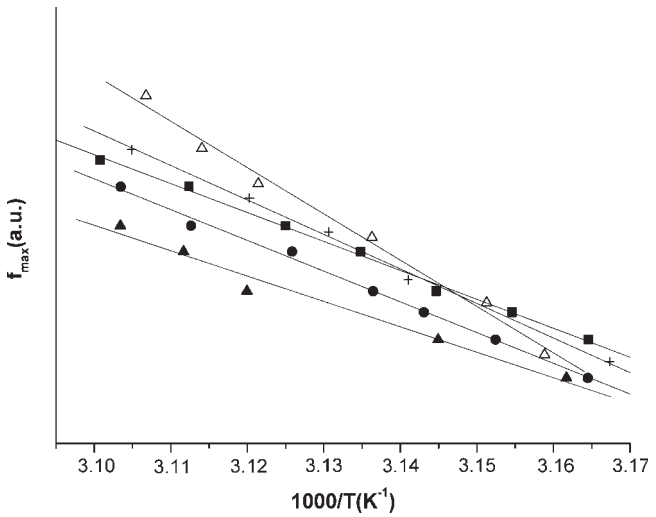

Figure 6 Arrhenius plots based on nonisothermal dielectric analysis for ODPG/MDA composites at several ODPG contents (wt %): ■ 57; ◆ 63; ▲ 67; △ 73; + 77. In this figure frequency is plotted on a l_n-scale against 1000/T. The slope of the linear fit is E_a/R.

curve, and f the frequency. The slope of the Arrhenius plot is $-E_a/R$. Activation energy for several compositions samples were calculated and presented in Table I.

The region around 70 wt % ODPG, related to the greatest values of E_a, corresponds to interval where the lowest dielectric loss values can be found. It is reasonable to assume that this region of ~70 wt % ODPG corresponds to greater energetic barrier of occurring motion of organic tethers (links between cubes).

These results of dielectric relaxation (ε'', E_a) are supported by those of the mechanical properties. This region of ~70 wt % ODPG corresponds to that

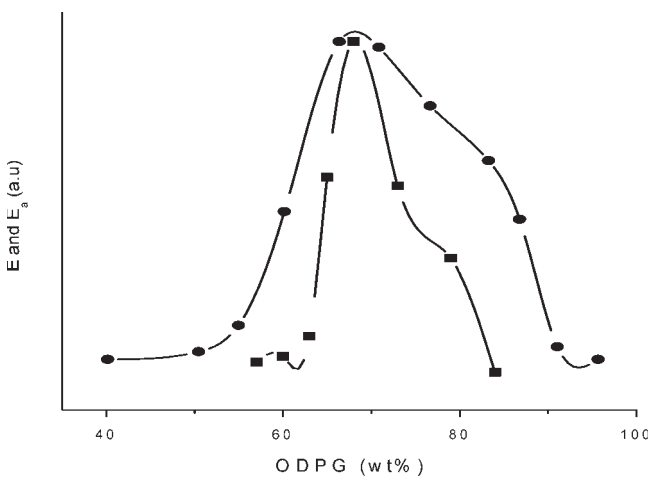

Figure 7 Comparison between the curves of activation energy (E_a) from DEA (■) and of tensile modulus mechanical property (E) (●) with respect to ODPG content (wt %).

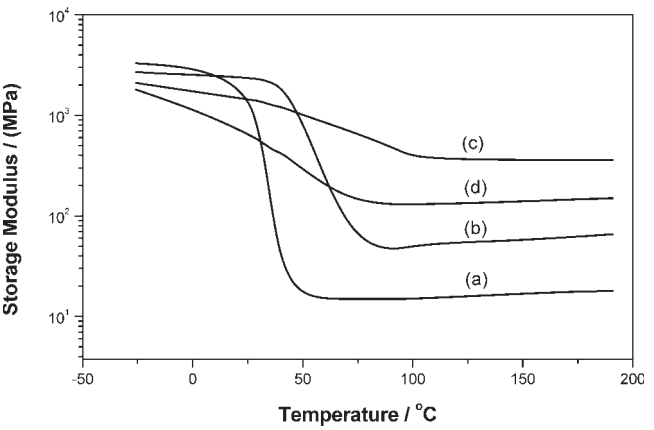

Figure 8 Storage modulus for ODPG/MDA composites at various ODPG contents (wt %): (a) 63, (b) 73, (c) 83, (d) 91.

presents the greatest Young modulus and fracture toughness values, as it is shown in Table I. The curves of activation energy (E_a) and of Young modulus (E) as a function of ODPG content, showed in the Figure 7, present the same profile with respect to ODPG content, in the sense that they exhibit maxima around 70 wt % ODPG. E_a obtained from DEA technique and E increased with increasing wt % ODPG up to around 70 wt %. Further increase in concentration of ODPG up to 83 wt % reduced E_a and E.

Figures 8 and 9 show the DMA of ODPG/MDA composites. In Figure 8 the maximum rubbery state modulus is found at $\phi = 1$. As the rubbery state modulus relates directly to the network crosslink density, the maximum crosslink density is expected at $\phi = 1$ (83 wt % OG and 17 wt % of MDA, corresponding to stoichiometric ratio), which appears in DMA as the maximum rubbery state modulus (Fig. 8) and the highest T_g (Fig. 9). It confirms that

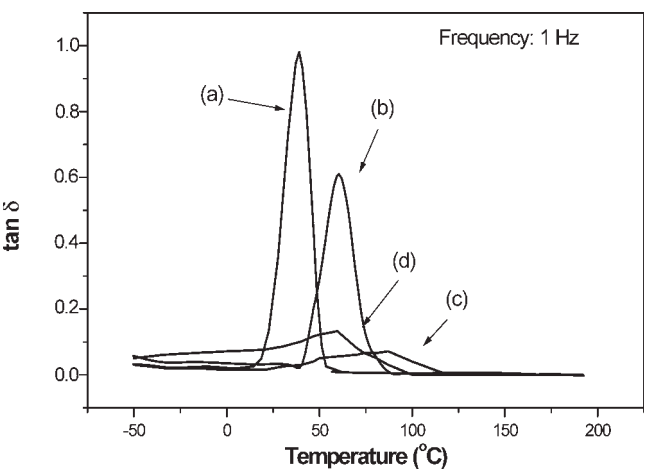

Figure 9 tan δ for ODPG/MDA composites at various ODPG contents (wt %): (a) 63, (b) 73, (c) 83, (d) 91.

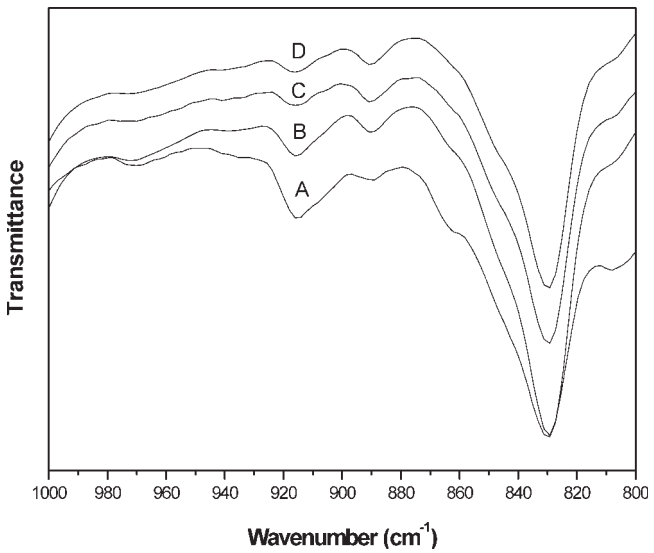

Figure 10 FTIR spectra for ODPG/MDA composites at various ODPG contents (wt %): (a) 83, (b) 77, (c) 73, (d) 67.

MDA acts as a tetrafunctional reactant in ODPG/MDA composites at $\phi = 1$. The small T_g peak in ODPG/MDA at $\phi = 1$ can be explained by a higher crosslink density this formulation. As the ODPG is octafunctional and the core is inorganic it provides extremely high crosslink densities in ODPG/MDA causing a high rubbery state modulus and the lack (small peak) of T_g.

Diffuse reflectance FTIR was used to follow the curing of various formulations. Figure 10 shows the expanded spectra from 800 to 1000 cm^{-1} for several ODPG/MDA composites with varying contents of ODPG. The epoxy ring symmetric stretching at ~830 cm^{-1} was present in all spectra but, practically, did not change its intensity. The epoxy ring asymmetric stretching at ~920 cm^{-1} was also present in all spectra and was used as an internal reference. The intensity this band decreases with increasing amounts of MDA is due to react on curing. This band at ~920 cm^{-1} remains even in the formulations with excess of MDA proving that the curing process presents residual cure.

It is known that for conventional epoxy resin, such as DGEBA, the highest crosslink densities are obtained at stoichiometries where two epoxy ring equivalents are mixed with one amine group equivalent (the ratio of epoxy ring to amine hydrogen is 1 : 1). Most epoxy thermoset materials exhibit the maximum Young modulus values for stoichiometries of $\phi = 1.0$ (ϕ is defined as the molar ratio of epoxy ring in conventional epoxy per amine hydrogen). Fracture toughness also increases as the amine content increases below $\phi = 1$. For the ODPG/MDA composites the highest crosslink density which is obtained at $\phi = 1$ implies that the dominating structure is expected to be the one in which MDA is tetrafunctional on curing, connecting four epoxy rings, and each cube has eight armed organic tethers (links between cubes).

On the contrary, for the ODPG/MDA composites, the maximum modulus and fracture toughness are obtained at $\phi \approx 0.50$, and they maintain their maxima modulus up to $\phi \approx 0.35$, which are not compositions where the highest crosslinked density are reached. This implies that the best mechanical properties are provided by some degree of chain flexibility.

This can be tentatively explained based on the fact that before occurring the complete reaction and crosslink between all the amines and epoxy rings, it becomes very difficult for unreacted functional groups to find each other because of increasing of the viscosity during curing. These unreacted functional groups will remain as pendant groups. Then, for $\phi < 1.0$, the excess increasing of MDA causes increased motion of organic tethers (links between cubes) by increasing the number of pendants groups and/or decreasing crosslink density. This α transition is caused by main chain motion. Other possibility is that the steric hindrance should be greater for bulky ODPG than for conventional epoxy, such as DGEBA. In this case, the reaction of the first hydrogen of the NH_2 group should be favored over the second one, resulting in a uniform and densely crosslinked structure that can be obtained at $\phi \approx 0.50$. In this case, the dominating structure is expected to be the one in which MDA is bifunctional on curing (linear tethers connecting two cubes). This assumption (MDA is bifunctional connecting two cubes) seems to be favored taking into consideration that the highest values of E_a obtained from DEA, E (tensile modulus), and K_{1C} (fracture toughness), occur in a ratio of ~4 mol of MDA to 1 mol of ODPG corresponding to $\phi \approx 0.50$.

For instance, when DGEBA is cured with excess MDA the material changes from ductile to a brittle material, both tensile modulus and fracture toughness increase from $\phi = 1.0$ to $\phi = 0.5$, and, then, they drop significantly.[11] Therefore, while epoxy resin/hardener conventional systems become brittle with excess of curing agent ($\phi < 1.0$), ODPG/MDA becomes rubbery. At $\phi < 0.14$, the modulus data of ODPG cannot be measured because of the rubber-like behavior. On the other hand, for composition at $\phi > 3.9$ (''Excess'' ODPG) the ODPG/MDA composites become viscous. Consequently, at $\phi > 3.9$, the modulus of ODPG/MDA cannot be measured, and no data points are included in Table I. This behavior also reflects in the fracture toughness, and no data points for $\phi < 0.44$ and $\phi > 1.0$ are included in Table I, because it is practically impossible to introduce a natural crack into these samples.

CONCLUSIONS

The dielectric properties of composites based on polyhedral oligomeric silsesquioxane epoxy resin, obtained by curing of 1,3,5,7,9,11,13,15-octa[dimethylsiloxypropylglycidylether] pentaciclo [9.5.1.1^{3,9}.1^{5,15}.1^{7,13}] octasilsesquioxane (ODPG), in presence of methylenedianiline (MDA) as hardener, was examined at various experimental conditions.

The dielectric loss maximum peak amplitude decreases with increasing ODPG content until about 70–73 wt % and slightly increases at higher ODPG content. This means that the increasing of the ODPG content in the composite samples decreases the number of pendants groups and/or increases crosslink density, causing decreased motion of organic tethers (links between cubes), and subsequently decreasing of the dipolar mobility.

The results of apparent activation energy, fracture toughness and tensile modulus mechanical properties show the same profile with respect to ODPG content, in the sense that they exhibit maxima around 70 wt % ODPG ($\phi \approx 0.50$). For the ODPG/MDA composites, this formulation of $\phi \approx 0.50$ containing excess of amine is not composition where the highest crosslinked density is reached. This implies that the best mechanical properties and E_a are provided by some degree of chain flexibility.

These results indicated that the dielectric technique can be used to know and to understand the relationships between the relaxational behavior, the ratio of oligomeric silsesquioxane epoxy resin to hardener, the structure of the networks, and the final properties of the composite matrix.

References

1. Voronkov, M. G.; Lavrent'yev, V. I. Top Curr Chem 1982, 102, 199.
2. Baney, R. H.; Itoh, M.; Sakakibara, A.; Suzuki, T. Chem Rev 1995, 95, 1409.
3. Provatas, A.; Matisons, J. G. Trends Polym Sci 1997, 5, 327.
4. Haddad, T. S.; Lichtenhan, J. D. Macromolecules 1996, 29, 7302.
5. Lichtenhan, J. D.; Otonari, Y. A.; Carr, M. J. Macromolecules 1995, 28, 8435.
6. Mantz, R. A.; Jones, P. F.; Chaffee, K. P.; Lichtenhan, J. D.; Gilaman, J. W.; Ismail, I. M. K.; Burmeister, M. J. Chem Mater 1996, 8, 1250.
7. Li, Z. G.; Wang, L.; Toghiani, H.; Daulton, T. L.; Pittman, C. U., Jr. Polymer 2002, 43, 4167.
8. Mya, Y. K.; He, C.; Huang, J.; Xiao, Y.; Dai, J.; Siow, P. Y. J Polym Sci Part A: Polym Chem 2004, 40, 3490.
9. Siegel, R. W.; Chang, S. K.; Ash, B. J.; Stone, J.; Ajayan, P. M.; Doremus, R. W.; Schadler, L. S. Scripta Mater 2001, 44, 2061.
10. Xu, R.; Manias, E.; Snyder, A. J.; Runt, J. Macromolecules 2001, 34, 337.
11. Dias Filho, N. L.; Laine, R. M.; Asuncion, M.; Baliat, S.; Harcup, J.; Sutorik, A. C.; Viculis, L.; Yee, A. F.; Zhang, C.; Zhu, Q. In Organic/Inorganic Hybrid Materials; Klein, L.; De Guire, M.; Lorraine, F.; Mark, J., Eds.; MRS Symposium Series, Vol. 576; American Chemical Society: Pittsburgh, PA, 1999; p 3.
12. Kranbuehl, D. E. In Dieletric Spectroscopy of Polymeric Materials: Fundamentals and Applications; Runt, J. P., Fitzgerald, J. J., Eds.; American Chemical Society: Washington, 1997; Chapter 11.
13. Prime, R. B. Thermal Characterization of Polymeric Materials, 2nd ed.; Academic Press: San Diego, 1997; Vol. 2, Chapter 6, p 1517.
14. Boyd, R. H. Polymer 1985, 26, 1123.
15. Ribelles, J. L. R.; Calleja, R. D. J Polym Sci Polym Phys Ed 1985, 23, 1297.
16. Huo, P.; Cebe, P. J Polym Sci Part B: Polym Phys 1992, 30, 239.
17. Dionísio, M. S.; Moura-Ramos, J. J.; Williams, G. Polymer 1994, 35, 1705.
18. Fitz, B. D.; Mijovic, J. Polym Adv Technol 1998, 9, 721.
19. Yi, H. Thermochim Acta 2001, 367/368, 101.
20. Valentini, L.; Puglia, D.; Frulloni, E.; Armentano, I.; Kenny, J. M.; Santucci, S. Compos Sci Technol 2004, 64, 23.